THE JOURNAL OF PHYSICAL CHEMISTRY A

pubs.acs.org/JPCA Article

Fate of Dipole-Bound Anion States when Hydrated

Iwona Anusiewicz, Piotr Skurski, and Jack Simons*

Cite This: J. Phys. Chem. A 2020, 124, 2064−2076 Read Online

ACCESS | Metrics & More | Article Recommendations

ABSTRACT: Many strongly polar molecules can form an anion by attaching an electron to either an empty or half-filled valence-bound (VB) orbital or a so-called dipole-bound (DB) orbital. These two families of orbitals can be very different in their radial extent (the former are usually more compact, while the latter are quite diffuse) and in the degree to which they are affected by surrounding solvent molecules. In this study, the effects of hydration (representative of strong solvation) on the DB state of a model polar species are investigated with an eye toward determining whether this state is stabilized or even persists when a few to 100 water molecules surround the polar molecule. It is found that in the presence of up to ca. 10−12 water molecules, the excess electron can remain in a DB orbital. However, once there are enough water molecules to form a complete first hydration shell (or more), the excess electron migrates into an orbital localized on the outer surface of the water solvent cage. These findings have implications on the possible role of DB states as doorways to facilitating electron attachment and subsequent electron transfer to VB states. It is shown that even when the electron is bound to the surface of the surrounding solvent, the dipole potential of the solute molecule can influence where on the surface the electron binds. It is also illustrated that using continuum dielectric methods to describe the hydration of DB states is fraught with danger because much of the outermost electron density in such states penetrates outside the boundary of the cavity used in these methods.

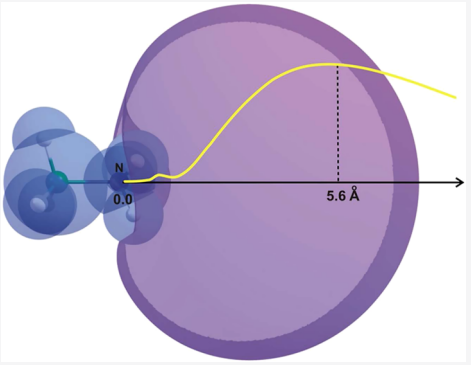

I. INTRODUCTION

For many years, it has been known and widely appreciated that molecules possessing large dipole moments (>ca. 2.5 D) can bind an electron via the attractive charge-dipole potential to produce a so-called dipole-bound (DB) anion. A review of such anionic states was provided by Jordan and Wang in 2003.[1] Of course, neutral molecules can also bind one or more excess electrons by attaching the electron(s) to a vacant or half-filled valence-type bonding, antibonding, or nonbonding orbital to form a so-called valence-bound (VB) anion. In fact, molecules can possess both VB and DB anionic states, and in Figure 1, we offer three examples from the recent literature of species for which both types of states exist and have been of considerable interest.

I.I. Examples of VB and DB Orbitals. In Figure 1A, we see the singly occupied orbitals that contain the excess electron in the π^* VB (top) and DB (bottom) states of the uracil anion, respectively.[2] In Figure 1B, we see the π^* VB (left) and DB (right) orbitals of the thymine anion−water complex,[3] and in Figure 1C, we see the DB (left) and π^* VB (right) orbitals of the Watson−Crick guanine−cytosine base−pair anion,[4] respectively.

The DB and VB anionic states can be very different in their stabilities relative to the energy of the neutral molecule. In particular, for all of the examples illustrated in Figure 1, near the equilibrium geometry of the neutral, the DB anion's energy lies below the neutral by a very small amount (e.g., a few tenths of an electronvolt or less). At these same geometries, the VB anion's energy lies above that of the neutral, which means that this state is metastable at those geometries. In contrast, near the equilibrium geometry of the VB anion, the VB state's energy lies below that of the neutral as does the DB state's energy. Moreover, the equilibrium geometry of the DB anion is very close to that of the neutral (because the DB orbital is essentially nonbonding and has most of its electron density far from the valence region), but the equilibrium geometry of the VB anion can differ substantially from that of the neutral (because the π^* VB orbital has significant antibonding character for the examples of Figure 1).

In Figure 2, we illustrate how the energies of the neutral and DB and VB anion states vary along transit paths connecting the neutral and VB anion geometries for the uracil[2] and GC dimer anion cases.[4] We emphasize two features of these slices through the multidimensional Born−Oppenheimer electronic energy surfaces of these species. First, as mentioned earlier, the VB state's energy lies above that of the neutral on the left-hand

Received: January 15, 2020
Revised: February 13, 2020
Published: February 17, 2020

https://dx.doi.org/10.1021/acs.jpca.0c00360
J. Phys. Chem. A 2020, 124, 2064−2076

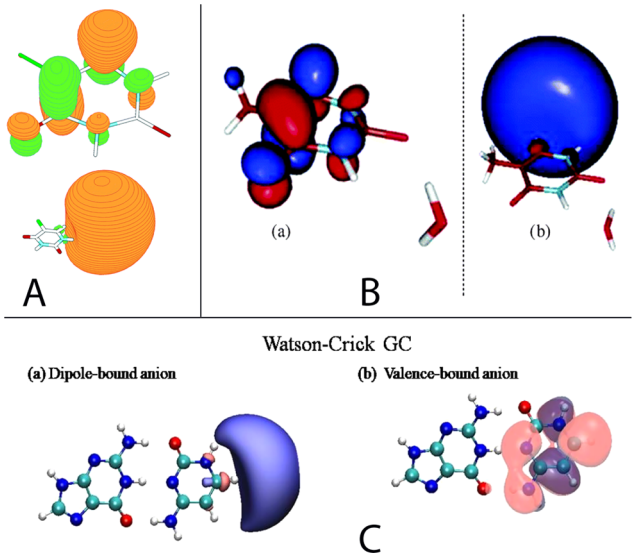

Figure 1. (A) Singly occupied orbitals of the valence (upper) and dipole-bound (lower) states of the uracil anion (from ref 2). (B) Singly occupied orbitals of valence-bound (a) and dipole-bound (b) thymine anion−water complex (from ref 3). (C) Singly occupied orbitals of (a) dipole-bound and (b) valence-bound Watson−Crick GC anion (from ref 4).

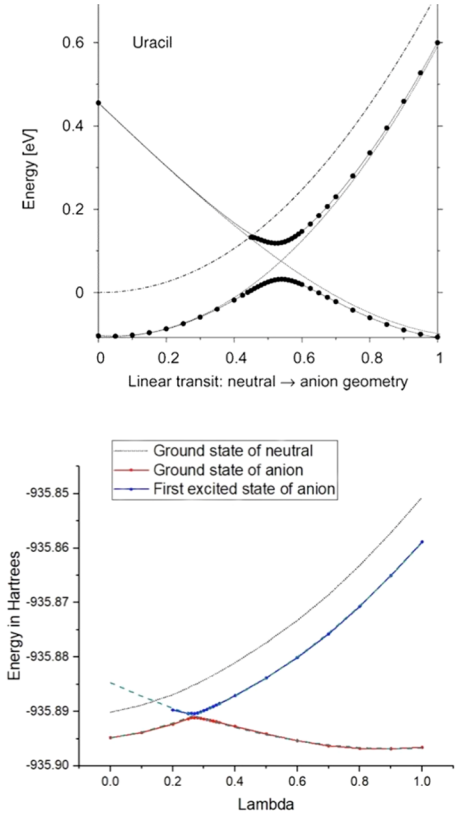

Figure 2. Cut through the energy surfaces of uracil and its two anionic states (top plot; from ref 2). The center curve on the left is the surface of the neutral, and the circles represent the two anionic states with the DB state being lower on the left and higher on the right where the VB state is lower. Cut through the energy surfaces for the Watson−Crick GC base pair and its anion with the DB curve lying below but parallel to the neutral and the VB curve being lowest on the right (bottom plot; from ref 4).

sides of these figures. This means that the evaluation of the VB state's energies at such geometries requires the use of specialized techniques (i.e., basis sets and tools for determining the lifetimes) that we will not discuss here as our main interest is in characterizing DB states and the effects of solvation on such states. Second, along the transit path, the energies of the DB and VB states approach one another and undergo avoided crossings. Not only does this mean that the DB state is the ground state at some geometries (e.g., on the left in the figures) while the VB state is the ground state at others (e.g., on the right), but it also means that there are geometries at which the two states are coupled. This latter fact means, for example, that an electron initially attached to the DB orbital at a geometry near that of the neutral can smoothly transition into the VB orbital if the DB anion's geometrical framework happens to access the neighborhood of the two states' avoided crossing.

I.II. Possibility of DB States Serving as Doorways to Forming VB States of the Anion. The fact that DB and VB states can approach near-degeneracy at geometries that might be accessed under various experimental conditions has been suggested by several workers[1,2,5−14] as a means through which DB could serve as doorways for accessing VB states when the neutral species collides with a free electron or with an electron donor having a small electron binding energy. Specifically, because the VB state lies above and is metastable relative to the energy of the corresponding neutral at such geometries, it is energetically favorable to attach an electron to form a DB anion and to then have internal vibrational motion of the nascent anion gain access to geometries at which the DB-to-VB electron transfer can occur. It is through such a process that the DB state has been proposed to serve as a doorway for forming the VB anion from the neutral molecule and a free or, for example, an electron in a Rydberg orbital of a donor. Of course, the efficiency of this mechanism will be governed by the height of the energy barrier (i.e., where the DB and VB states' energy undergo the avoided crossing) and the coupling strength between the DB and VB states (i.e., the strength of the avoided crossing). Although it is reasonable to expect that DB states can provide a doorway to VB states for an isolated polar molecule, it is not clear to what extent this possibility persists when the polar molecule exists in condensed media or when a few to many solvent molecules surround the polar molecule.

I.III. What Happens If There Are Solvent Molecules around the Polar Solute Molecule? First, let us make it clear what we are not trying to determine in this study. We are not attempting to characterize the lowest-energy (or free-energy) state of a polar molecule and an excess electron in the presence of a few, several, or many solvent molecules. That avenue would be appropriate to pursue if we were interested in what happens after the excess electron had attached and the geometries of the solute molecule and of the surrounding solvent molecules had time to relax to a new low-energy equilibrium.

Instead, we want to know what could happen when an electron (free or bound to a donor anion) collides with a polar molecule that has a few, several, or many solvent molecules arranged around it in a structure that is low in energy for this neutral species. It is under such environments that the suggestion of dipole-bound states serving as doorways to the subsequent formation of valence-bound states arises because the doorway state is assumed to be formed before the solute

https://dx.doi.org/10.1021/acs.jpca.0c00360
J. Phys. Chem. A 2020, 124, 2064−2076

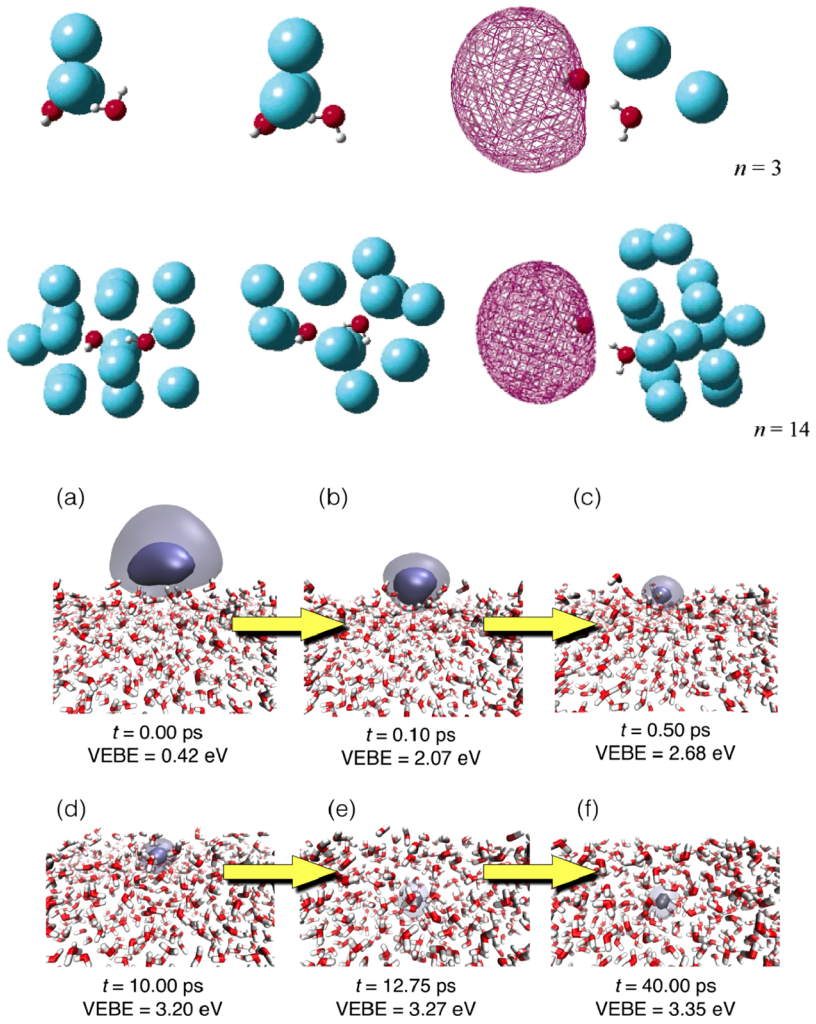

Figure 3. Depictions of neutral trans-$(H_2O)_2$ Ar_{14} (left, top) and cis-$(H_2O)_2Ar_{14}$ (middle, top), and anionic $(H_2O)_2^-Ar_{14}$ (right, top) (from ref 15) and of the evolution of a surface-bound electron into an interior-bound electron (bottom) (from ref 16).

and surrounding solvent have had time to undergo geometry relaxation.

To illustrate these distinctions between geometrically unrelaxed and relaxed conditions, we now offer a brief discussion of two studies from other labs involving an electron, a polar species, and a few to many solvent molecules. In 2004, Tsai et al.[15] carried out a study of electron attachment to a water dimer $(H_2O)_2$ with 1−14 Ar atoms bound to it. The water dimer has a large enough dipole moment to bind an electron, so it is viewed as the dipolar species, while the Ar atoms are viewed as the (weakly solvating) solvent species. Monte-Carlo and simulated annealing methods were used to identify minimum-energy locations of the Ar atoms relative to the water dimer and the water dimer anion. In Figure 3 (top), we see six snapshot depictions of the resulting structures for (left) the neutral trans-water dimer, (middle) the neutral cis-water dimer, and (right) the water dimer anion, each solvated by 3 or 14 Ar atoms. The cis-dimer has a dipole moment of 4.02 D, and the trans-isomer's dipole moment is 2.49 D, so both are capable of dipole binding an excess electron. It is clear from Figure 3 that the solvent molecules are arranged very differently in the neutral and anion cases when there are many Ar atoms present. For Ar_{14}, the Ar atoms surround the neutral water dimer, while in the anion, the Ar atoms cluster away from the dipole-bound electron. In contrast, for Ar_3, the Ar atoms reside in similar angular locations in both the neutral and anionic water dimers. Thus, for $(H_2O)_2Ar_3$ at or near the geometry of the neutral complex, there exist water O−H bonds extending outward that can act to form a dipole-bound anion as seen on the right-most figure for Ar_3. In contrast, for $(H_2O)_2Ar_{14}$ at or near the geometry of the neutral complex, there is no room for the dipole-bound orbital to form. As a result, the 14 Ar atoms must substantially rearrange to permit the formation of the dipole-bound state as seen on the right-most figure for Ar_{14}. As will be shown later, analogous situations arise in the systems we are studying here.

In the bottom portion of Figure 3, we show a depiction taken from the work of Coons et al.[16] of the orbital occupied by an excess electron in the presence of many water molecules at an air−water interface. In that work, the initial (t = 0) solvent molecules' positions were chosen as a snapshot taken from an equilibrated (300 K) simulation (including periodic boundary conditions) of neat water. At such a geometry, the existence of O−H bonds protruding outward from the water−air interface produces a sufficient local dipole potential to bind an excess electron. The orbital initially occupied by the electron in this case is shown in panel (a) and corresponds to a dipole-bound state having an electron binding energy of 0.42 eV. As time evolves over tens of picoseconds, the molecular dynamics simulation whose results are given in Figure 3 shows

https://dx.doi.org/10.1021/acs.jpca.0c00360
J. Phys. Chem. A 2020, 124, 2064−2076

that the water molecules reorient and rearrange to change the initially surface-bound electron into an interior cavity-bound electron as seen in panels (e) and (f).

In the case of $(H_2O)_2Ar_{14}$, the addition of an excess electron causes the solvation environment to evolve in a manner that allows an exterior dipole-bound state to be energetically preferred, but this evolution would require picoseconds to take place and thus would not occur if a free electron were to encounter $(H_2O)_2Ar_{14}$ at the geometry of the neutral complex. The electron−complex collision event would not endure long enough for the 14 Ar atoms to move into the locations needed to form a dipole-bound state.

In the second case, the addition of an excess electron causes the solvation environment to evolve away from a surface dipole-bound state into an interior cavity-bound state, again over picoseconds. The formation of the initial state could occur if a free electron were to encounter the neat water surface shown in Figure 3a because the orbital relaxation needed to accommodate the excess electron would have time to take place. However, the interior-bound state existing at t = 40 ps would not be formed directly by an electron impacting the neat t = 0 water surface; it would have to form as described in Figure 3 by the nascent surface-bound state undergoing substantial solvent reorganization over tens of picoseconds.

In the present work, we want to study what happens when an excess electron attaches to a solvated neutral polar molecule within the very short time span (<1 ps) during which the solvent and solute's orbitals have sufficient time to adjust but during which the solvent and solute's geometries do not have time to adjust to the presence of the excess electron. We view this as the proper way to explore whether, within the time frame significantly shorter than that needed for major or full solvent rearrangement, a free electron, or one weakly bound to a donor, would attach in a dipole-bound manner to a polar molecule that has solvent molecules around it.

With the above explanation in mind, let us now outline the strategy we used to probe the basic question how, if at all, will an excess electron bind to a polar molecule if that neutral polar molecule has a few to many water molecules around it in locations that correspond to a low total energy of the neutral? The polar molecule we chose to use is the Lewis base−acid complex H_3BNH_3 (denoted X in the following), which has a dipole moment of 5.356 D. To characterize the surrounding solvent, we used $(H_2O)_N$ clusters containing 10, 12, 20, 40, or 100 H_2O molecules initially arranged into closed cages that possess little to no dipole moment. These solvation environments were selected to allow us to be sure that most of the dipole moment of the species with H_3BNH_3 inside the water cage arises from the polar solute molecule. These cages are also somewhat representative of how a polar molecule would exist in a low-energy state in the presence of several water molecules. In Table 1, we list the dipole moments for each of the empty cages and for the cages with the H_3BNH_3 inside. These data clearly show that only the N = 10 empty cage has an appreciable dipole moment and the dipole moments of the $H_3BNH_3(H_2O)_n$ species are very nearly equal to the sum of the dipole moment of the H_3BNH_3 solute plus that of the empty cage. The latter results mean that the presence of the solute does not induce any significant dipole moment in the cage's water molecule framework.

Table 1. Dipole Moments (Debyes) for Empty Water Cages and for Cages with H_3BNH_3 Inside

cage size	empty $(H_2O)_N$ cage	$H_3BNH_3(H_2O)_N$
N = 10	2.5580	6.989
N = 12	0.0214	5.116
N = 20	0.0350	5.265
N = 40	0.0037	5.214
N = 100	0.0710	5.076

These highly symmetrical initial water cage structures were also allowed to undergo geometrical relaxation to better accommodate the internal neutral solute molecule and to reach a lower-energy state. As will be illustrated later, the hydrogen-bond networks present in the unrelaxed $(H_2O)_N$ clusters we employ are more icelike than liquid-water-like. But, by also examining the geometrically relaxed cages, we are able to explore a slightly broader distribution of solvation environments, and we believe the crowding environments included in the unrelaxed and relaxed cages are qualitatively representative of both liquid and ice situations.

For both the initial and relaxed cages, one excess electron was added and the orbitals of the solute and water cage molecules were allowed to relax to accommodate the excess electron. However, for the reasons explained earlier relating to the nature of the electron attachment process we are studying, further geometrical relaxation of the solute or water solvent molecules' geometries after the excess electron was attached was not permitted. The singly occupied molecular orbital (SOMO) of each such anion was then used to characterize the nature, dipole-bound or not, of the binding of the excess electron.

II. METHODS

The equilibrium structure and the corresponding harmonic vibrational frequencies of the isolated neutral H_3NBH_3 molecule were determined by applying the second-order Møller−Plesset (MP2) perturbational method[17−19] with the aug-cc-pVDZ[20] basis set supplemented with a 5s5p4d set of diffuse functions centered on the nitrogen atom (since this is the centroid of the positive end of the dipole). The extra diffuse functions do not share exponent values, and we used even-tempered[21] five-term s, five-term p, and four-term d basis sets. The geometric progression ratio was equal to 3.2,[22] and, for each symmetry, we started to build up the exponents of the extra diffuse functions from the lowest exponent of the same symmetry included in aug-cc-pVDZ basis set designed for nitrogen. As a consequence, we achieved the lowest exponents of 1.825×10^{-4}, 1.672×10^{-4}, and 2.193×10^{-3} au, for the s, p, and d symmetries, respectively. We examined the lowest eigenvalue of the atomic orbital overlap matrix to determine that near-linear dependency was not a problem. Since we determined that the MP2 electron binding energy for the $H_3NBH_3^-$ anion increases by less than 1 cm^{-1} after inclusion of an additional set of diffuse 2s2p1d functions (leading to 7s7p5d diffuse set), and by less than 3 cm^{-1} after replacing the aug-cc-pVDZ + 5s5p4d basis with the aug-cc-pVTZ + 5s5p4d, we are confident that our final basis set was selected to be the aug-cc-pVDZ basis supplemented with the 5s5p4d diffuse set for the optimization of geometries, for calculating frequencies, and for evaluating the electron binding energies (at the Koopmans theorem[23] (KT) and the MP2 levels).

The $(H_2O)_{10}$, $(H_2O)_{12}$, $(H_2O)_{20}$, $(H_2O)_{40}$, and $(H_2O)_{100}$ water clusters were chosen to surround the H_3NBH_3 molecule because (i) $(H_2O)_{10}$ and $(H_2O)_{12}$ seem to represent the

https://dx.doi.org/10.1021/acs.jpca.0c00360
J. Phys. Chem. A 2020, 124, 2064−2076

smallest solvation shell sufficiently large to fully encapsulate the H_3NBH_3 molecule and (ii) the remaining $(H_2O)_N$ structures (N = 20, 40, and 100) correspond to icosahedral (thus exhibiting relatively high symmetry) clusters in which the first solvation shell is stabilized by additional layers of H-bonded water molecules. Our choice of such icosahedral water clusters was also guided by the fact that such structures possess nearly vanishing dipole moments and hence would not be expected to increase the dipole-induced electron binding energy beyond that generated by H_3NBH_3. Therefore, it seemed reasonable to perform only single-point energy calculations on the $(H_2O)_N$ clusters containing H_3NBH_3 in their centers (i.e., for the geometrically unrelaxed (i.e., with the $(H_2O)_N$ clusters' geometries unchanged) neutral $X(H_2O)_N$ systems, where N = 10, 12, 20, 40, 100).

Taking into account the substantial size of the largest system considered ($H_3NBH_3(H_2O)_{100}$ contains 102 heavy atoms and 206 hydrogen atoms), we had to limit these cluster calculations to the Hartree−Fock level. In these calculations, we applied the aug-cc-pVDZ + 5s5p4d basis for H_3NBH_3 (as described in the preceding paragraph) and the 6−31++G(d,p) basis set[24,25] for the N water molecules.

To prepare plots of the molecular orbitals such that their outer contours contain 80% of the orbital's electron density, we employed the OpenCubMan software described and created by Harańczyk et al.[26]

The lowest unoccupied molecular orbitals (LUMO) of the neutral $X(H_2O)_N$ systems and the SOMOs of their corresponding $X(H_2O)_N^-$ anions were obtained at the $X(H_2O)_N$ neutral structures by converging the self-consistent-field (SCF) procedure in the absence of or with one additional electron, respectively, keeping the neutral molecule's geometry frozen. The KT energy of the LUMO orbital produces an electron affinity (EA) estimate that does not account for relaxation of the occupied orbitals of the $X(H_2O)_N$, whereas the KT energy of the SOMO provides an EA estimate that does account for such orbital relaxation. These differences are important to note because they relate to the high-frequency dielectric response of the solute and solvent upon the addition of the excess electron. As will be seen shortly, the LUMOs and SOMOs of some species are very similar, but for others, they differ significantly. For the reasons explained earlier, the kind of electron attachment processes that we are attempting to address would occur over time frames within which the orbitals of the nascent anion would have time to adjust. Therefore, it is the SOMOs and their energies that are of the most relevance to this study.

Finally, we also examined solvent effects beyond the shells of explicit solvent molecules included in the cages by employing the polarized continuum solvation model (PCM)[27−29] within a self-consistent reaction field treatment, as implemented in the GAUSSIAN16 (Rev. C.01) package[30] (the default options for PCM and dielectric constants (ε) of 2 and 78 were used). For reasons that are explained later, we did not expect such a continuum solvation approach to succeed, but we wanted to use the dipole-bound species studied here to illustrate why one should not employ such methods in cases characterized by very diffuse electron densities.

III. RESULTS AND DISCUSSION

III.I. DB State of the Model Solute X. We chose to employ H_3NBH_3 as a solute because (i) it has a large enough dipole moment (5.356 D) to support a DB state but has no low-energy valence-bound anion state (thus allowing us to focus totally on the behavior of the dipole-bound state), and (ii) its dipole moment is large enough that its Koopmans' theorem (KT) electron affinity (EA) is without doubt positive[31] even though we know[32−34] that correlation is likely to increase the EA value. That is, we did not have to employ highly correlated calculations to achieve a qualitatively correct description of the DB state of interest.

In Figure 4, we show the LUMO of the neutral H_3NBH_3 and the SOMO of the $H_3NBH_3^-$ anion with the outermost contour

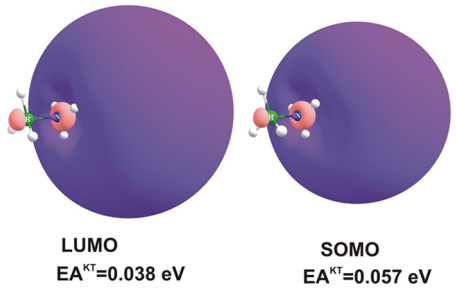

Figure 4. LUMO of the neutral isolated H_3NBH_3 and the SOMO of the isolated $H_3NBH_3^-$ anion. The B atom is colored green, and the N atom is blue.

containing 80% of the electron density (in all subsequent orbital plots, this same 80% density will apply). Of course, in the case of the LUMO and for all LUMOs discussed here, the density refers to the density that would be present if the orbital were actually occupied. The neutral molecule LUMO KT-level EA of this species (EA^{KT}) is 0.038 eV, the anion's SOMO electron detachment energy is 0.057 eV, and at a highly correlated level,[31] the detachment energy is 0.122 eV.

The difference between the LUMO and SOMO electron binding energies arises from the H_3NBH_3 molecule's orbital relaxation present in the latter and absent in the former and is what gives rise to the size contraction of the SOMO relative to the LUMO.

III.II. Neutral Solute X within Various-Size Water Cages. Focusing on what happens to the DB state when the X species is surrounded by molecules with a high dielectric constant, we carried out ab initio calculations in which the solvation environment consists of a cage of N H_2O molecules arranged in such a way that the cage itself (i.e., without the X molecule being present) has little dipole moment of its own. The structures of the $(H_2O)_{10}$ and $(H_2O)_{12}$ clusters were retrieved from The Cambridge Cluster Database,[35] whereas the remaining icosahedral structures of $(H_2O)_N$ (N = 20, 40, 100) were taken from ref 36.

In Figures 5 and 6, we show the structures of the $X(H_2O)_N$ for N = 10, 12, 20, 40, and 100, and for each case, we show the dipole moment vector (directed from positive to negative). The magnitudes of the dipole moments were given earlier in Table 1. It should be noted that the geometries of the water molecules within the $X(H_2O)_N$ have not been optimized; they are the geometries for the bare $(H_2O)_N$ cages taken from the sources cited above. The X solute molecule was simply placed at the center of the cage in each case, with no attempt to optimize its location.

Notice that for all five caged species, the dipole vector is directed along the N−B bond axis as expected because the cages have small dipole moments. Also, note that for the N = 10 and 12 cages, there appears to be one intact solvation shell,

https://dx.doi.org/10.1021/acs.jpca.0c00360
J. Phys. Chem. A 2020, 124, 2064−2076

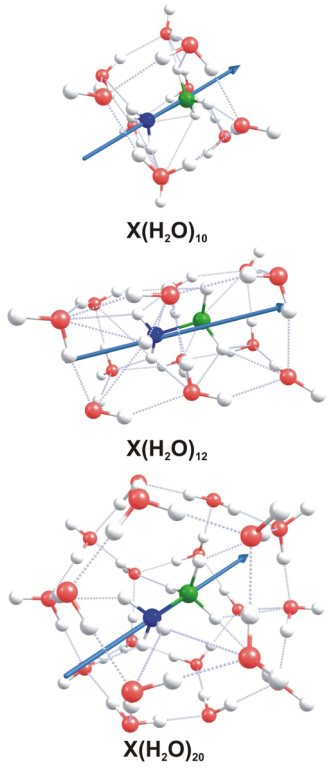

Figure 5. Structures of the neutral $X(H_2O)_{10}$, $X(H_2O)_{12}$, and $X(H_2O)_{20}$.

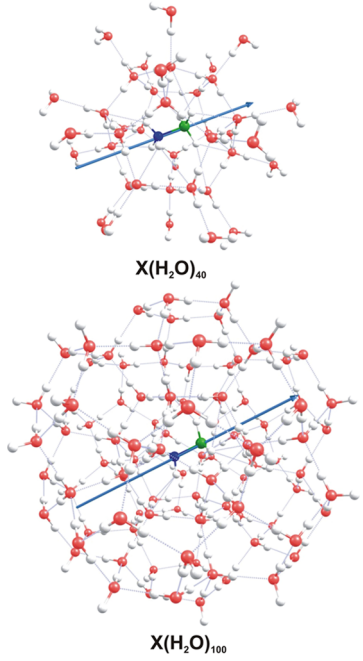

Figure 6. Structures of the neutral $X(H_2O)_{40}$ and $X(H_2O)_{100}$.

while for the $N = 20$ cage, there are two shells, and for the $N = 40$ and 100 cages, there are three or more solvation shells.

As noted earlier, the H_2O molecules within each cage are by no means oriented to optimally solvate the X molecule. Nevertheless, the cages do provide the solvent "crowding" that we are attempting to examine in this study as well as a series of shells of H_2O molecules arranged in reasonable hydrogen-bonded networks.

To consider the possibility that the $(H_2O)_N$ cages were too small to accommodate the neutral X molecule in a reasonably low-energy environment, we carried out geometry relaxation studies on the $N = 10$, 12, 20, and 40 cages. The relaxed structures of these $X(H_2O)_N$ species and their dipole moment vectors are shown in Figure 7. Comparing the original and

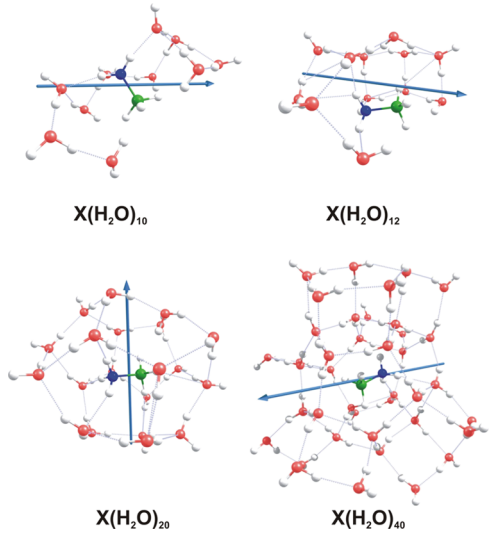

Figure 7. Geometrically relaxed structures of $X(H_2O)_{10}$, $X(H_2O)_{12}$, $X(H_2O)_{20}$, and $X(H_2O)_{40}$.

relaxed structures, we note that (i) for $N = 10$ and 12, the water cages appear to undergo substantial reorganization, to disconnect their innermost hydration layer, and to no longer fully surround the solute molecule, while (ii) for $N = 20$ and 40, the hydration layers appear to remain intact and the solute molecule remains surrounded even though the cages have undergone substantial geometry changes, especially in their hydrogen bonding network, as we will discuss in Section III.V.

Another thing to note about the relaxed structures is that their dipole moment vectors are significantly different from those of the original structures. These changes result from the $(H_2O)_N$ cages developing substantial dipole moments of their own as their geometries are allowed to adjust to the presence of the solute molecule. Finally, for the $N = 10$ and 12 relaxed structures, the water molecules have rearranged in a manner that leaves the NH_3 end of the solute molecule exposed.

III.III. Evolution of the DB (or Not!) States of the Caged Species. In Figure 8, we display the KT LUMOs of the unrelaxed (i.e., using the geometries in Figures 5 and 6) $X(H_2O)_N$ species for $N = 10$, 12, 20, 40, and 100 along with the corresponding KT EA values. We do not show the SOMOs of the corresponding $X(H_2O)_N^-$ anions because, much like in Figure 4, they are very similar to (but slightly smaller than) the LUMOs we show. However, we do display the SOMO KT EA values to give an idea of the extent to which the solute and solvent orbital relaxation contributes. Recall that for all five of these species, the dipole moment is directed along the N−B bond axis, so any DB state resulting from the dipole potential of X should be aligned in this direction.

In Figure 8, it is clear that for $N = 10$ and 12, the orbital is localized mostly along the N−B bond direction and on the positive H_3N side of the dipole. However, for $N = 20$, 40, and 100, the LUMO is not localized along this direction. We interpret this to mean that the DB state might persist for the N

https://dx.doi.org/10.1021/acs.jpca.0c00360
J. Phys. Chem. A 2020, 124, 2064−2076

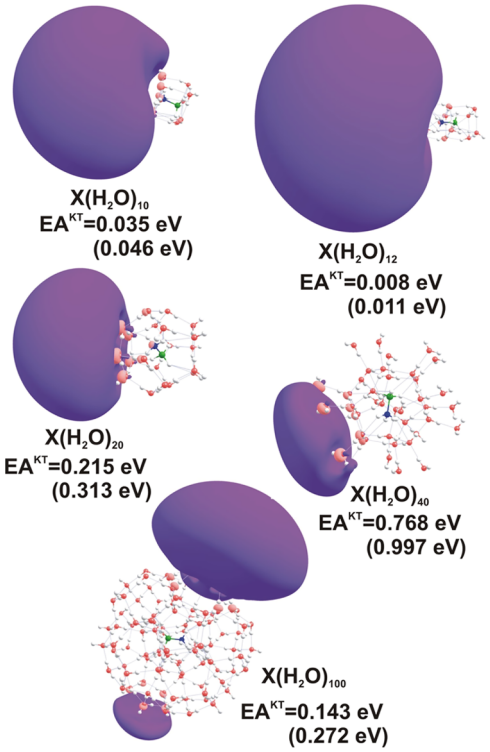

Figure 8. LUMOs for the neutral unrelaxed $X(H_2O)_{10}$, $X(H_2O)_{12}$, $X(H_2O)_{20}$, $X(H_2O)_{40}$, and $X(H_2O)_{100}$ and the corresponding KT EAs (in electronvolts). For comparison, the SOMO-derived EAs are given in parentheses.

= 10 and 12 cage species but is not present for the N = 20, 40, and 100 cage species. In the latter cases, the LUMO consists of an orbital localized and bound on the periphery of the $(H_2O)_N$ cage. This interpretation is also supported by the KT EAs shown in Figure 8; those for the N = 10 and 12 cages are close to that of the bare X solute (0.038 eV), whereas those for N = 20, 40, and 100 are considerably larger.

We also note that for the three larger cage systems, where X is surrounded by two or more solvent shells, the LUMO's primary density is separated from the X molecule by one or more shells of H_2O molecules. In further support of the claim that the DB state appears to disappear, we examined several of the higher-energy virtual orbitals (i.e., LUMO + 1, LUMO + 2, etc., both bound and unbound) of $X(H_2O)_{20}$, $X(H_2O)_{40}$, and $X(H_2O)_{100}$ and found no sign of a DB-like orbital.

In addition to the DB state not persisting beyond one solvation shell of H_2O molecules, Figure 8 shows that the distance from the center of the X solute species to the centroid of either the DB (for N = 10 and 12) or cage surface-bound (N = 20, 40, and 100) orbital increases as the cage grows. Much of this increase is due to the presence of intervening H_2O molecules. This distance increase would be expected to decrease the rates of doorway DB-to-VB electron transfer in species that possess both types of states even if one were to suggest that surface-bound (SB) states such as those shown above might serve as doorways to the SB-to-VB electron transfer. This possibility would, of course, be pertinent to experiments carried out on very small $X(H_2O)_N$ clusters. However, when considering the solute X within a macroscopic water droplet or in bulk aqueous solution, the above findings suggest that the DB state will have disappeared so there would exist no DB doorway state to undergo electron transfer to the VB anion.

III.IV. Do the Cage Surface-Bound States Arise from the Cage or from the X Molecule? For N = 20, 40, and 100, we carried out calculations on the corresponding clusters in which the electrons and nuclei of the X molecule were removed (but all of the basis orbitals used in the calculations discussed above were retained; the basis functions of X were positioned where the nuclei of X had originally been located). This strategy allowed us to consider the possibility that the SB states result from the electrostatic potential generated by the cages and not from any potential generated by the X molecule.

In Figure 9, we show the LUMOs for the unrelaxed N = 20, 40, and 100 empty cages. In our opinion, the three LUMOs of

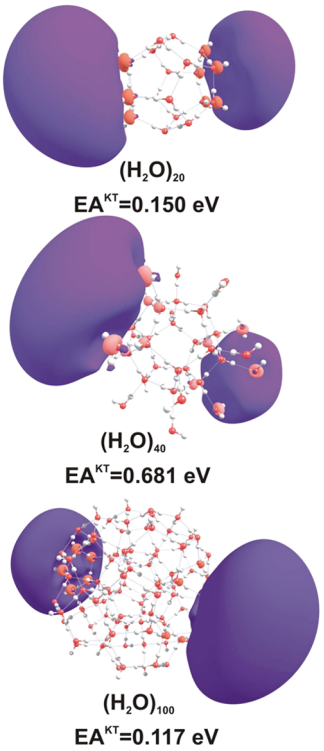

Figure 9. LUMOs and EAs for the empty $(H_2O)_{20}$, $(H_2O)_{40}$, and $(H_2O)_{100}$ cages having the aug-cc-pVDZ basis centered on all ghost atoms plus the 5s5p4d set of diffuse functions centered on a ghost atom (where the N atom was originally located) inside the cage.

these empty cages are similar in shape, radial size, and electron binding energy to those shown in Figure 8 for the corresponding $X(H_2O)_N$ species but with two small but significant differences. First, for the empty cages, the LUMOs all have two lobes, one on each side of the cage, and second, the EAs of the empty cages are all slightly (ca. 0.1 eV) smaller than the EAs of the systems with X inside the cage. The fact that the empty cages all have essentially zero dipole moments yet still bind the excess electron more tightly than does the bare X^- anion suggests that the cages are effecting their electron binding by making use of their several O−H bonds that are directed outward from the center of the cage. Note that these three cages all possess such O−H bonds in both regions where the LUMOs have their lobes. The fact that the EAs of the species with X inside are all somewhat larger than those of the empty cages suggests that the dipole potential of the X molecule is somewhat enhancing the attractive potential

https://dx.doi.org/10.1021/acs.jpca.0c00360
J. Phys. Chem. A 2020, 124, 2064−2076

of the cages' outward-directed O−H bonds. In support of this latter claim, we note that the LUMOs of the $X(H_2O)_N$ all have only one lobe and that lobe lies on the side where the X molecule's positive NH_3 unit sits.

In summary, with respect to how the excess electron is bound to the unrelaxed N = 20, 40, and 100 empty and filled cages, we think it is appropriate to conclude that these states derive primarily from the interaction of the excess electron with the outward-directed O−H bonds' electrostatic potentials of the cages with the attractive dipole potential of the X molecule adding little to the EA. In further support of this conclusion, we examined several of the higher-energy virtual orbitals (i.e., LUMO + 1, LUMO + 2, etc., bound and unbound) of the $X(H_2O)_N$ and $(H_2O)_N$ species and found the empty cages' orbitals to be very similar to those of the full systems' orbitals.

III.V. What about for the Relaxed Cages? Earlier, we noted that the geometries of the N = 10 and 12 $X(H_2O)_N$ complexes undergo substantial relaxation and open up their inner hydration shells when the X solute molecule is present. Although the N = 20 and 40 complexes retain intact inner (and more) hydration layers, they do still undergo substantial reorganization of their hydrogen bonding networks. What happens to the EA values and what can we say about what is governing these values?

Recall that the unrelaxed cages had essentially zero dipole moments, that the X molecule has a dipole moment of 5.356 D, and that the dipole moments of the $X(H_2O)_N$ complexes were close to 5.4 D for N = 12, 20, 40, and 100. In Table 2, we show the dipole moments of the N = 10, 12, 20, and 40 empty relaxed cages along with the corresponding values with the X molecule inside the cages.

Table 2. Dipole Moments (Debyes) for Relaxed Empty Water Cages and for Relaxed Cages with H_3BNH_3 Inside

cage size	empty $(H_2O)_N$ cage	$H_3BNH_3(H_2O)_N$
N = 10	6.851	6.101
N = 12	2.210	6.868
N = 20	8.477	5.372
N = 40	1.449	5.418

Clearly, the empty cages now possess substantial dipole moments while the filled cages have total dipole moments that differ significantly from the corresponding empty cage values. Moreover, the cage dipole vectors are not collinear with that of the X molecule inside the cage. If we assume that the total dipole moment $\boldsymbol{\mu}_{Tot}$ of each $X(H_2O)_N$ species is the sum of the dipole moment $\boldsymbol{\mu}_X$ of the X molecule and the dipole moment $\boldsymbol{\mu}_{Cage}$ of the cage, we can estimate the angle $\boldsymbol{\theta}$ between the N−B bond axis and the direction of the total dipole moment vector using the law of cosines

$$(\boldsymbol{\mu}_{Cage})^2 = (\boldsymbol{\mu}_X)^2 + (\boldsymbol{\mu}_{Tot})^2 - 2\,\boldsymbol{\mu}_{Tot}\boldsymbol{\mu}_X \cos\boldsymbol{\theta} \quad (1)$$

For the N = 10, 12, 20, and 40 systems, this calculation yields $\boldsymbol{\theta}$ = 73, 15, 104, and 16°, respectively. Then, through the law of sines, one can evaluate the angle ϕ between the dipole moment vector of the empty cage and the N−B bond axis. For the N = 10, 12, 20, and 40 systems, this calculation yields $\boldsymbol{\phi}$ = 58, 54, 38, and 83°, respectively. We are interested in these vector orientations because we want to determine whether the total dipole potential or that of the cage is influential in determining where the excess electron binds.

In Figure 10, we show the SOMO orbitals and their KT electron binding energies for the relaxed N = 10, 12, 20, and 40 $X(H_2O)_N^-$ anions.

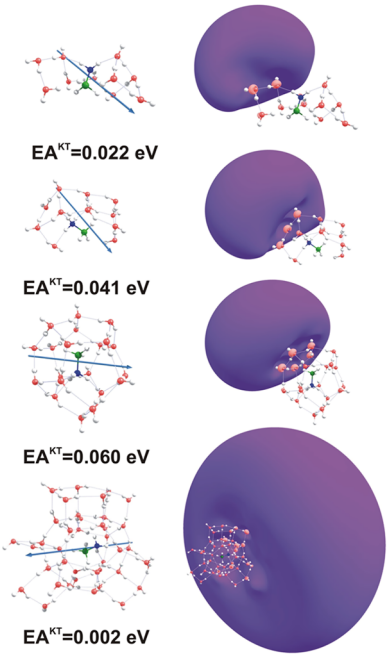

Figure 10. SOMOs and structures for the relaxed $X(H_2O)_{10}^-$, $X(H_2O)_{12}^-$, $X(H_2O)_{20}^-$, and $X(H_2O)_{40}^-$, and the corresponding KT EAs (in electronvolts). In each case, the structure and SOMO pictures hold the N−B bond axis in the same orientation, and in each case, the direction of the total dipole moment vector is shown.

In all four cases, we see that the SOMO is oriented along the total dipole moment vector and not along either the B−N bond axis or the dipole moment of the empty cage. This is especially clear for the N = 10 and 20 systems where the angles between the total dipole vector and the B−N bond axis are 73 and 104°, respectively, and the dipole of the empty cages lie 58 and 38° off the direction of the B−N bond axis. Another thing to note is that the SOMOs are localized in regions of space where the cages have outward-directed O−H bonds, a fact that contributes to the total dipole moment's magnitude and direction.

All of the relaxed systems have EAs that are typical of dipole binding, but the preceding paragraph should make it clear that it is not the dipole of the X species that is dominating in the binding. An interesting contrast exists between the unrelaxed and relaxed systems for N = 20 and 40. For the relaxed species, the SOMOs have EAs (0.040 and 0.002 eV) that are much smaller than those of the corresponding unrelaxed clusters (0.313 and 0.768 eV; see Figure 8) even though the total dipole moments of these pairs of species are quite similar (see Tables 1 and 2). When examining the structures of the N = 20 and 40 unrelaxed systems (see Figures 5 and 6), we note that they possess not only outward-directed O−H bonds but water molecules in which both O−H bonds are so directed (i.e., water molecules that are referred to as double acceptors AA of hydrogen bonds from neighboring water molecules). It has been shown[44] that such AA sites provide strong attraction to an excess electron. Although we cannot say for certain, we

https://dx.doi.org/10.1021/acs.jpca.0c00360
J. Phys. Chem. A 2020, 124, 2064−2076

suggest that it is the presence of AA sites in the unrelaxed N = 20 and 40 species that are not present in the corresponding relaxed species that gives rise to the substantial increases in EAs in the former.

III.VI. Can Continuum Models Be Used to Describe Solvent Effects on DB States? *III.VI.I. Strong Solvation of the Bare X and X⁻ Solutes.* Although we anticipated that continuum solvation methods would not work well on dipole-bound states for reasons that we provide later, it was not as clear to us that similar limitations would arise to the same extent for the SB states. To illustrate the difficulties that we expected, we now examine what happens if one uses the polarized continuum model (PCM)[27−29] to describe the effect of solvation on the DB state of the neutral X or the X^- anion. In such continuum dielectric models, a cavity is formed within which the solute of interest exists and a model potential on the surface of the cavity and outside it is then used to characterize the effect of the surrounding solvent. In the present case, we chose to model equilibrium solvation in which the solvent molecules are located, oriented, and polarized to experience the presence of the X or X^- solute. In Figure 11, we show the

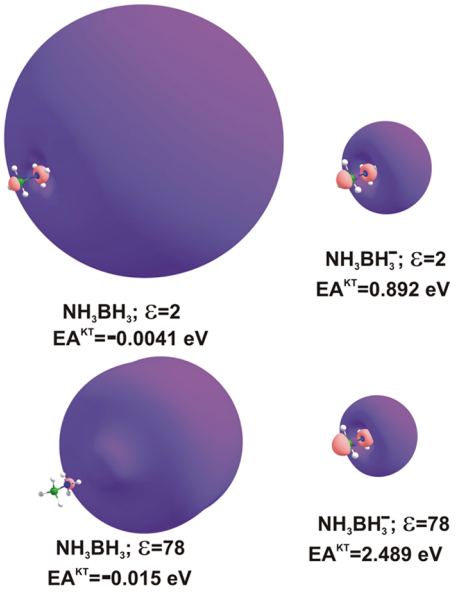

Figure 11. LUMOs for neutral H_3NBH_3 and SOMOs for the $H_3NBH_3^-$ anion for ε = 2 and 78 (see Figure 4 for the ε = 1 orbitals).

LUMO for neutral X and the SOMO of anionic X^- using dielectric constants of ε = 2 (representative of a hydrocarbon or approximating the high-frequency dielectric response of water) and 78 (water). Figure 4 shows the corresponding orbitals for the ε = 1 (gas phase) case.

The LUMO orbitals and their KT EA values are expected to relate to the attachment of an electron to a H_3NBH_3 molecule surrounded by solvent molecules arranged and oriented in a manner appropriate to solvating this neutral molecule but not accounting for any orbital relaxation or reorientation of the solute or solvent. In contrast, the SOMO orbitals are expected to relate to a DB $H_3NBH_3^-$ anion surrounded by solvent molecules arranged and oriented in a manner appropriate to solvating this negatively charged species, and thus the SOMO KT EA values should relate to the energy needed to remove an electron from this equilibrium-solvated anion. For these reasons, one expects the LUMO and SOMO KT EA values to be very different, as they are for the two ε values whose results are shown in Figure 11.

We see that the LUMO-based KT EA values for both ε = 2 and 78 are negative, suggesting that attachment of an excess electron to the neutral solvated X would be endothermic unless orbital relaxation of the complex were sufficient to render it exothermic. In addition, we note that the PCM potential, which is designed to model solvation of the neutral X species, acts to destabilize the LUMO (i.e., the LUMO-based EA values change from 0.038 to −0.004 to −0.015 eV as ε increases from 1 to 2 to 78). In contrast, the SOMO-based EA values are both positive and larger than for the gas-phase case and range from 0.057 to 0.892 to 2.489 eV as ε increases from 1 to 2 to 78. This means that the PCM potential acts to stabilize the SOMO.

So, unlike what we found for the bare X and X^- and for the $X(H_2O)_N$ and $X(H_2O)_N^-$ complexes where the LUMOs and SOMOs and their corresponding EA values were similar, once the PCM potential is applied, the LUMOs and SOMOs are very different. This might not be surprising because the PCM potential is different for the neutral and anionic species. For the issue we are addressing—attaching a free electron to a solvated neutral polar molecule—the result most likely to be of any relevance would be the SOMO for ε = 2 because this dielectric constant could approximate the high-frequency response of the water solvent.

To help understand why it is unwise to trust the above SOMO-based results derived from applying PCM directly to X and X^-, we show in Figure 12 two pictures of the DB SOMO

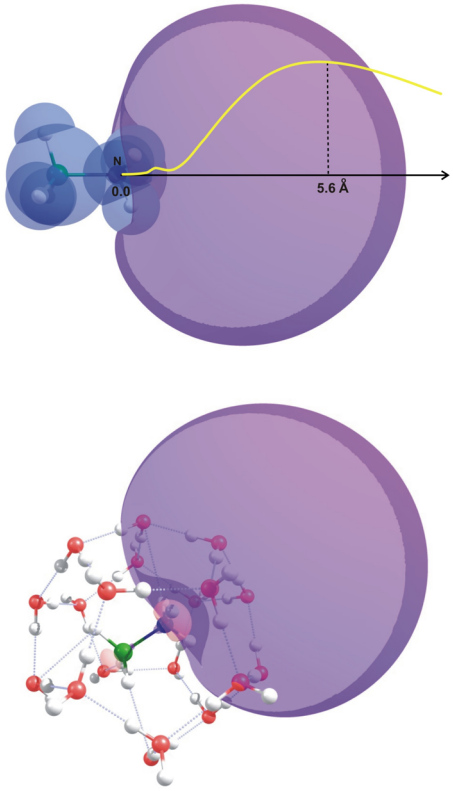

Figure 12. X^- and its dipole-bound orbital superimposed onto a depiction of the underlying X molecule's van der Waals surface (top) and inserted into the center of the unrelaxed $(H_2O)_{20}$ cage (bottom). In the former, the maximum in the DB orbital's density is shown to occur ca. 5.6 Å to the right of the N atom.

https://dx.doi.org/10.1021/acs.jpca.0c00360
J. Phys. Chem. A 2020, 124, 2064−2076

of the bare X^-: (i) first, with its SOMO superimposed on a depiction of the van der Waals surface of the underlying neutral X molecule and (ii) next with the X^- species and its SOMO simply inserted into the center of the unrelaxed $(H_2O)_{20}$ cage. In the top picture, we also plot the radial density profile[37] of the DB orbital that has its maximum 5.6 Å to the right of the N atom and extends beyond the outermost blue contour (recall that our orbital plots show the volume within which 80% of the electron density resides). These pictures are designed to illustrate the degree to which the electron density of the DB orbital would penetrate beyond the cavity boundary defined in terms of van der Waals radii (top picture) and into the network of the surrounding water molecules if it were to remain intact (bottom picture). In our opinion, such a DB orbital would have to be strongly stabilized, and thus radially contracted, to fit within such a cavity even if the cavity were to surround the $(H_2O)_{20}$ cage.

In continuum dielectric solvation models, the solute molecule or ion is assumed to exist within a cavity[38] whose size and shape are determined, for example, by tracing out the van der Waals (vdW) radii of the constituent atoms or by tracing the outermost contour of the solute's electron density at some specified iso-density value. Because DB anions possess significant electron density (i.e., most of the entire excess electron) in regions far from the underlying atoms' vdW radii, a vdW-based cavity would exclude much of the DB orbital's density. Alternatively, using a very low iso-density value to create a cavity that would contain most of the DB orbital's density might generate a cavity that does not fit properly near the H_3B group. As Figure 12 (top) illustrates, in the PCM calculations whose results are shown in Figure 11, the cavity enclosed the full van der Waals surface of the X molecule but did not enclose much of the space occupied by the DB orbital. For this reason, such a continuum dielectric treatment of the bare X and X^- species should not be trusted because such models assume that not much electron density penetrates beyond the boundary of the cavity it uses.

Figure 12 (bottom) suggests that, even if a DB orbital were to persist when X^- was surrounded by as many as 20 H_2O molecules, even the van der Waals surface of that $X^-(H_2O)_{20}$ cluster would not be large enough to enclose most of the DB orbital's electron density.

It should be noted that the authors of ref 16, whose results were discussed earlier, pointed out the difficulties in applying continuum solvation methods to the surface-bound state (see the bottom image of Figure 3a) because the excess electron's density extends substantially beyond any reasonable cavity boundary. In contrast, in that same article, the authors were able to apply continuum solvation to the interior-bound electron state (see the bottom image of Figure 3f). In 2015, Kumar et al.[39] also were successful in using such methods to describe the solvation of $(H_2O)_N^-$ cluster anions with N = 4, 6, and 16 when the water molecules were constrained to form closed cavities within which the excess electron was trapped. In that case and in the interior-bound case of ref16, essentially all of the electron density resided inside the border of the cavity which is why the continuum solvation methods were successful. However, as we will now demonstrate, using such methods on our $X(H_2O)_N^-$ clusters will not succeed because their excess electron's density protrudes too far beyond the cavity boundary.

III.VI.II. Using PCM on $X(H_2O)_N^-$ Clusters. Looking at Figure 12 and keeping in mind that continuum dielectric theories need to construct a cavity that contains most of the electron density of the system, one might expect to not succeed even by including 20 explicit water molecules and then attempting to treat the remaining solvation using PCM. That is, the DB orbital is expected to extend beyond the range of van der Waals surface of the 20 explicit water molecules. For this reason, we decided to also explore adding 40 explicit water molecules and then using PCM to approximate further solvation anticipating possible failure for N = 20 and possible success for N = 40.

In Figure 13, we show the SOMOs and their KT EA values for $X(H_2O)_{20}$ and $X(H_2O)_{40}$ for ε = 2 and 78, respectively.

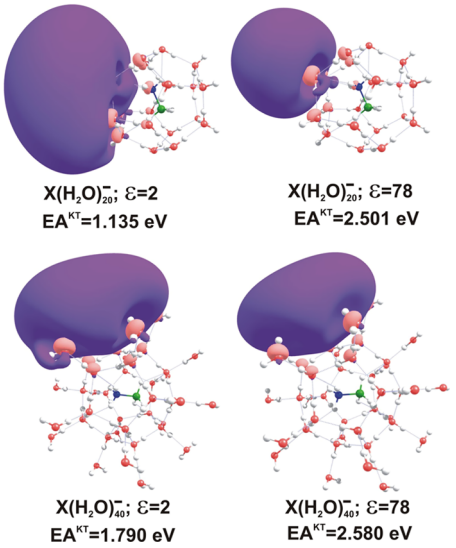

Figure 13. SOMOs for the $X(H_2O)_{20}^-$ and $X(H_2O)_{40}^-$ anions obtained with PCM for ε = 2 and 78.

As was the case for PCM solvation of bare X and X^-, we find that the PCM potential stabilizes the SOMO and more so for ε = 78 than for ε = 2. Importantly, in the presence of the PCM potential, the excess electron does not remain in a DB-like orbital but, instead, migrates to the surface of the N = 20 or 40 cluster much like we found (see Figure 8) for the $X(H_2O)_{20}$ and $X(H_2O)_{40}$ clusters when no PCM potential was operative. Even though the N = 20 and 40 orbitals shown in Figure 13 are similar to those shown in Figure 8, where no PCM potential was present, the EA values in Figure 13 are very much larger than those in Figure 8.

It is worth noting that we tried to offer the excess electron a good chance to form a dipole-bound state inside the clusters by initiating the self-consistent field orbital optimization process using the dipole-bound orbital of the bare X^- anion as the first approximation to the converged orbital. We thought this would maximize the chance for the final optimized orbital to have a significant amplitude within the cages rather than on the periphery. However, even with such an initial orbital approximation, the SCF orbital optimization eventually produced the surface-bound orbitals shown in Figure 13.

Thus, the strategy of including 10−40 explicit water molecules in the model system and then using PCM to treat solvation effects outside the $X(H_2O)_N^-$ complex does not succeed because the resulting $X(H_2O)_N^-$ complexes also have much electron density penetrating beyond the boundary of the cavity the PCM model creates even when the cavity includes the van der Waals space occupied by the 10−40 surrounding

https://dx.doi.org/10.1021/acs.jpca.0c00360
J. Phys. Chem. A 2020, 124, 2064−2076

water molecules. So, we also conclude that it is not appropriate to employ such models to treat solvation of surface-bound anionic states of the $X(H_2O)_N^-$ clusters. One could argue that the particular continuum dielectric model embodied within the PCM method we chose could be replaced by a better model. For example, the SVPE method of Chipman[40,41] provides an improved description of the solvation beyond the boundary of the cavity. However, because the DB and SB anions have so much of their outmost electron density extending far beyond the van der Waals surface boundary, we think it is unlikely that any continuum dielectric model could adequately describe the actual solvation that is present in the bulk or in the kind of clusters we studied here.

IV. CONCLUSIONS

The ab initio electronic structure calculations reported here suggest that:

1. The existence of a DB state likely can survive the presence of a few to several nearby solvent molecules, as evidenced by the results on $X(H_2O)_{10}^-$ and $X(H_2O)_{12}^-$ shown in Figures 8 and 10, on the thymine−water complex shown in Figure 1B, and on $(H_2O)_2Ar_3$ shown in Figure 3. This suggests that experimental probes of lightly solvated DB species could produce, for example, spectroscopic signature characteristic of DB states. However, it is important to be aware of what such signatures are. For a dipole-bound state, the photodetachment spectra should display a very narrow progression of vibrational structures because the geometry change arising from removing the excess electron should be small. However, it is not proper to assume that the electron detachment energy itself must be small (i.e., <0.1 eV). As we see in Figure 10 for the relaxed species, the excess electron is bound to the total dipole of the complex by a small amount, whereas, for the unrelaxed structures shown in Figure 8, the electron can be bound by nearly 1 eV. In ref 16 and in work by Uhlig et al.,[42] it was found that surface-bound electrons and electrons held internally in water molecule cages can have very similar and large (i.e., tenths of electronvolts) binding energies. The point is that the magnitude of the EA need not be a reliable factor upon which to determine dipole binding.
2. Once the number of solvent molecules is sufficient to surround the putative DB species and form a solvation network whose internal intermolecular interactions render it stable, the DB state likely disappears. When water is the solvent, as in this work, it is energetically favorable to arrange the H_2O molecules in a maximally hydrogen-bonded network than to have some of the H_2O molecules surround and solvate the DB orbital. In such cases, the excess electron prefers to be bound to the surface of the solvation cage that surrounds the neutral solute molecule if the cage itself produces a sufficiently attractive potential (as the $(H_2O)_N$ cages were shown to do for N = 10, 12, 20, 40, and 100). This suggests that experimental probes of somewhat more heavily solvated putative DB species would produce signatures not characteristic of a dipole-bound state of X^- but of a surface-bound (SB) state of the solvent cage.
3. For the degree of explicit solvation considered here, there is no evidence that the DB state persists by occupying interstices within the solvent cages; instead, it evolves into an SB state once one or more full solvation shells exist. This does not mean that the excess electron cannot be bound in a more interior manner (e.g., as in solvated-electron clusters containing hundreds of water molecules[16,42,43] or as in charge-transfer-to-solvent (CTTS) cases) when even more solvent molecules are present. As mentioned earlier, the unrelaxed water clusters we chose to employ possess hydrogen-bond networks that are more icelike. Certainly, liquidlike water cluster structures could provide more interstices, but we do not believe that even in this case could there exist sufficient such space to allow the full DB orbital to persist.
4. The SB states in $X(H_2O)_{20}^-$, $X(H_2O)_{40}^-$, and $X(H_2O)_{100}^-$ arise primarily from the attractive potential exerted on the excess electron by the cage itself rather than by the polar X molecule inside the cage although the dipole potential of X does play a role in determining which side of the $(H_2O)_N$ cage the excess electron binds to. For the unrelaxed cages, the X dipole moment favors binding to one side of the highly symmetric cage; for the relaxed cages, the X dipole combines with the cage dipole to produce a total dipole that guides the excess electron toward its positive end.
5. Some of the icelike unrelaxed water cages employed here possess several outer-layer H_2O molecules whose two O−H bonds are directed outward (i.e., so-called AA water molecules). In such cases, the surface-bound EA values turned out to be large (i.e., several tenths of an electronvolt), which is not surprising given the experimental spectroscopic data[44] emphasizing the importance of such AA surface H_2O molecules in forming SB states. The corresponding relaxed water cages did not possess such AA water molecules and, as a result, had considerably smaller EA values.
6. As the number of surrounding solvent molecules grows, the distance from the SB orbital to the X solute species increases. This makes it less and less likely, as N increases, for the SB state to serve a doorway for electron transfer into a valence-bound state of X.
7. It is not proper to describe the effects of solvation of a bare DB X^- ion using continuum dielectric models because the DB orbital's electron density extends too far beyond the surface of the cavity defined by these solvation models. It is also not proper to describe the effects of solvation of the $X(H_2O)_N^-$ anions studied here using continuum dielectric models because the SB orbitals of such species also extend substantially beyond the cavity boundary created by the solvation model for these systems. In contrast, continuum solvation methods can be used successfully when the excess electron is held within a solvent-molecule cage as was shown in refs 16, 39.

AUTHOR INFORMATION

Corresponding Author

Jack Simons − *Henry Eyring Center for Theoretical Chemistry, Department of Chemistry, University of Utah, Salt Lake City, Utah 84112, United States;* orcid.org/0000-0001-8722-184X; Email: jack.simons@utah.edu

https://dx.doi.org/10.1021/acs.jpca.0c00360
J. Phys. Chem. A 2020, 124, 2064−2076

Authors

Iwona Anusiewicz − *Laboratory of Quantum Chemistry, Faculty of Chemistry, University of Gdańsk, 80-308 Gdańsk, Poland;* orcid.org/0000-0002-7506-8427

Piotr Skurski − *Laboratory of Quantum Chemistry, Faculty of Chemistry, University of Gdańsk, 80-308 Gdańsk, Poland; Henry Eyring Center for Theoretical Chemistry, Department of Chemistry, University of Utah, Salt Lake City, Utah 84112, United States*

Complete contact information is available at: https://pubs.acs.org/10.1021/acs.jpca.0c00360

Notes

The authors declare no competing financial interest.

■ ACKNOWLEDGMENTS

This research was supported by the Polish Ministry of Science and Higher Education Grant no. DS 531-8375-D499-19 (to P.S.). The calculations have been carried out using resources provided by Wroclaw Centre for Networking and Supercomputing (http://wcss.pl) Grant nos. 435 and 455. The authors also acknowledge several helpful communications with Dr. Daniel M. Chipman concerning continuum dielectric treatments of solvation.

■ REFERENCES

(1) Jordan, K. D.; Wang, F. Theory of Dipole-Bound Anions. *Annu. Rev. Phys. Chem.* **2003**, *54*, 367−396.

(2) Sommerfeld, T. Intramolecular Electron Transfer from Dipole-Bound to Valence Orbitals: Uracil and 5-Chlorouracil. *J. Phys. Chem. A* **2004**, *108*, 9150−9154.

(3) Frigato, T.; Svozil, D.; Jungwirth, P. Valence- and Dipole-Bound Anions of the Thymine-Water Complex: Ab Initio Characterization of the Potential Energy Surfaces. *J. Phys. Chem. A* **2006**, *110*, 2916−2923.

(4) Tripathi, D.; Dutta, A. K. Electron Attachment to DNA Base Pairs: An Interplay of Dipole- and Valence-Bound States. *J. Phys. Chem. A* **2019**, *123*, 10131−10138.

(5) Millar, T. J.; Walsh, C.; Field, T. A. Negative Ions in Space. *Chem. Rev.* **2017**, *117*, 1765−1795.

(6) Liu, G.; Ciborowski, S. M.; Ross Pitts, C.; Graham, J. D.; Buytendyk, A. M.; Lectka, T.; Bowen, K. H. Observation of the Dipole- and Quadrupole-Bound Anions of 1,4-dicyanocyclohexane. *Phys. Chem. Chem. Phys.* **2019**, *21*, 18310−18315.

(7) Bull, J. N.; Verlet, J. R. R. Observation and Ultrafast Dynamics of a Nonvalence Correlation-Bound State of an Anion. *Sci. Adv.* **2017**, *3*, No. e1603106.

(8) Frigato, T.; Svozil, D.; Jungwirth, P. Valence- and Dipole-Bound Anions of the Thymine-Water Complex: Ab Initio Characterization of the Potential Energy Surfaces. *J. Phys. Chem. A* **2006**, *110*, 2916−2923.

(9) Middleton, C. T.; de La Harpe, K.; Su, C.; Law, Y. K.; Crespo-Hernández, C. E.; Kohler, B. DNA Excited-State Dynamics: From Single Bases to the Double Helix. *Annu. Rev. Phys. Chem.* **2009**, *60*, 217−239.

(10) Stokes, S. T.; Grubisic, A.; Li, X.; Ko, Y. J.; Bowen, K. H. Photoelectron Spectroscopy of the Parent Anions of the Nucleotides, Adenosine-5′-Monophosphate and 2′-Deoxyadenosine-5′-Monophosphate. *J. Chem. Phys.* **2008**, *128*, No. 044314.

(11) Sommerfeld, T. Dipole-Bound States as Doorways in (Dissociative) Electron Attachment. *J. Phys.: Conf. Ser.* **2005**, *4*, 245−250.

(12) Ptasińska, S.; Denifl, S.; Grill, V.; Mark, T. D.; Scheier, P.; Gohlke, S.; Huels, M. A.; Illenberger, E. Bond-Selective H^- Ion Abstraction from Thymine. *Angew. Chem., Int. Ed.* **2005**, *44*, 1647−1650.

(13) Voora, V. K.; Jordan, K. D. Nonvalence Correlation-Bound Anion State of C_6F_6: Doorway to Low-Energy Electron Capture. *J. Phys. Chem. A* **2014**, *118*, 7201−7205.

(14) Rogers, J. P.; Anstoter, C. S.; Verlet, J. R. R. Ultrafast Dynamics of Low-Energy Electron Attachment via a Non-Valence Correlation-Bound State. *Nat. Chem.* **2018**, *10*, 341−346.

(15) Tsai, M.-K.; Wang, F.; Jordan, K. D. Electron Attachment to $(H_2O)_2Ar_n$ Clusters. *J. Phys. Chem. A* **2004**, *108*, 2912−2921.

(16) Coons, M. P.; You, Z.-Q.; Herbert, J. M. The Hydrated Electron at the Surface of Neat Liquid Water Appears To Be Indistinguishable from the Bulk Species. *J. Am. Chem. Soc.* **2016**, *138*, 10879−10886.

(17) Møller, C.; Plesset, M. S. Note on an Approximation Treatment for Many-Electron Systems. *Phys. Rev.* **1934**, *46*, 618−622.

(18) Head-Gordon, M.; Pople, J. A.; Frisch, M. J. MP2 Energy Evaluation by Direct Methods. *Chem. Phys. Lett.* **1988**, *153*, 503−506.

(19) Frisch, M. J.; Head-Gordon, M.; Pople, J. A. A Direct MP2 Gradient Method. *Chem. Phys. Lett.* **1990**, *166*, 275−280.

(20) Kendall, R. A.; Dunning, T. H., Jr; Harrison, R. J. Electron Affinities of the First-Row Atoms Revisited. Systematic Basis Sets and Wave Functions. *J. Chem. Phys.* **1992**, *96*, 6796−6806.

(21) Schmidt, M. W.; Ruedenberg, K. Effective Convergence to Complete Orbital Bases and to the Atomic Hartree-Fock Limit Through Systematic Sequences of Gaussian Primitives. *J. Chem. Phys.* **1979**, *71*, 3951−3962.

(22) Gutowski, M.; Simons, J. Double-Rydberg Anions: Ground-State Electronic and Geometric Stabilities. *J. Chem. Phys.* **1990**, *93*, 3874−3880.

(23) Koopmans, T. The Classification of Wave Functions and Eigenvalues to the Single Electrons of an Atom. *Physica* **1934**, *1*, 104−113.

(24) McLean, A. D.; Chandler, G. S. Contracted Gaussian Basis Sets for Molecular Calculations. I. Second Row Atoms, Z = 11-18. *J. Chem. Phys.* **1980**, *72*, 5639−5648.

(25) Krishnan, R.; Binkley, J. S.; Seeger, R.; Pople, J. A. Self-Consistent Molecular Orbital Methods. XX. A Basis Set for Correlated Wave Functions. *J. Chem. Phys.* **1980**, *72*, 650−654.

(26) Harańczyk, M.; Gutowski, M. Visualization of Molecular Orbitals and the Related Electron Densities. *J. Chem. Theory Comput.* **2008**, *4*, 689−693.

(27) Miertuš, S.; Scrocco, E.; Tomasi, J. Electrostatic Interaction of a Solute with a Continuum. A Direct Utilization of Ab Initio Molecular Potentials for the Prevision of Solvent Effects. *Chem. Phys.* **1981**, *55*, 117−129.

(28) Miertuš, S.; Tomasi, J. Approximate Evaluations of the Electrostatic Free Energy and Internal Energy Changes in Solution Processes. *Chem. Phys.* **1982**, *65*, 239−245.

(29) Cossi, M.; Barone, V.; Cammi, R.; Tomasi, J. Ab Initio Study of Solvated Molecules: A New Implementation of the Polarizable Continuum Model. *Chem. Phys. Lett.* **1996**, *255*, 327−335.

(30) Frisch, M. J.; Trucks, G. W.; Schlegel, H. B.; Scuseria, G. E.; Robb, M. A.; Cheeseman, J. R.; Scalmani, G.; Barone, V.; Petersson, G. A.; Nakatsuji, H. et al. *Gaussian 16*, revision C.01; Gaussian, Inc.: Wallingford, CT, 2016.

(31) Barrios, R.; Skurski, P.; Rak, J.; Gutowski, M. An Ab Initio Study of $(H_3B{\leftarrow}NH_3)^-$ - a Dipole-Bound Anion Supported by the Dative Charge-transfer Bond in the Neutral Host. *J. Chem. Phys.* **2000**, *113*, 8961−8968.

(32) Gutowski, M.; Skurski, P.; Boldyrev, A. I.; Simons, J.; Jordan, K. D. Contribution of Electron Correlation to the Stability of Dipole-Bound Anionic States. *Phys. Rev. A* **1996**, *54*, 1906−1909.

(33) Gutowski, M.; Skurski, P.; Jordan, K. D.; Simons, J. Energies of Dipole-Bound Anionic States. *Int. J. Quantum Chem.* **1997**, *64*, 183−191.

(34) Gutowski, M.; Jordan, K. D.; Skurski, P. Electronic Structure of Dipole-Bound Anions. *J. Phys. Chem. A* **1998**, *102*, 2624−2633.

(35) Maheshwary, S.; Patel, N.; Sathyamurthy, N.; Kulkarni, A. D.; Gadre, S. R. Structure and Stability of Water Clusters $(H_2O)_n$, n = 8-

20: An Ab Initio Investigation. *J. Phys. Chem. A* **2001**, *105*, 10525−10537.
(36) Loboda, O.; Goncharuk, V. Theoretical Study on Icosahedral Water Clusters. *Chem. Phys. Lett.* **2010**, *484*, 144−147.
(37) Lu, T.; Chen, F. Multiwfn: A Multifunctional Wavefunction Analyzer. *J. Comput. Chem.* **2012**, *33*, 580−592.
(38) For the Gaussian Program that We Use, this Issue is Discussed (and References are Given) at: https://gaussian.com/scrf/ (accessed Jan 15, 2020).
(39) Kumar, A.; Walker, J. A.; Bartels, D. M.; Sevilla, M. D. A Simple Ab Initio Model for the Hydrated Electron That Matches Experiment. *J. Phys. Chem. A* **2015**, *119*, 9148−9159.
(40) Zhan, C.-G.; Bentley, J.; Chipman, D. M. Volume Polarization in Reaction Field Theory. *J. Chem. Phys.* **1998**, *108*, 177−192.
(41) Chipman, D. M. Comparison of Solvent Reaction Field Representations. *Theor. Chem. Acc.* **2002**, *107*, 80−89.
(42) Uhlig, F.; Herbert, J. M.; Coons, M. P.; Jungwirth, P. Optical Spectroscopy of the Bulk and Interfacial Hydrated Electron from Ab Initio Calculations. *J. Phys. Chem. A* **2014**, *118*, 7507−7515.
(43) Verlet, J. R. R.; Bragg, A. E.; Kammrath, A.; Cheshnovsky, O.; Neumark, D. M. Observation of Large Water-Cluster Anions with Surface-Bound Excess Electrons. *Science* **2005**, *307*, 93−96.
(44) Hammer, N. I.; Shin, J.-W.; Headrick, J. M.; Diken, E. G.; Roscioli, J. R.; Weddle, G. H.; Johnson, M. A. How Do Small Water Clusters Bind an Excess Electron? *Science* **2004**, *306*, 675−679.

https://dx.doi.org/10.1021/acs.jpca.0c00360
J. Phys. Chem. A 2020, 124, 2064−2076